----- Forwarded Message -----
From: Емилия Машиах <ctbloan@nacid.bg>
To: veselin paunov <veskopaunov@yahoo.com>
Sent: Wednesday, April 10, 2013 10:40 AM
Subject: Re: otnosno zayavka v NACID-CNTB za statia

Уважаеми господин Паунов,
Изпращам Ви в прикачен файл доставената статия. Парите са получени в нашето счетоводство и те са длъжни да Ви издадат фактура. Бихте ли ми изпратили данни за фактура!?
Ако имате и други въпроси, не се безпокойте да ми пишете.
Приятен ден!
Емилия Машиах

From: veselin paunov
Sent: Friday, March 29, 2013 7:39 PM
To: Емилия Машиах
Subject: Re: otnosno zayavka v NACID-CNTB za statia

Zdraveite, usloviata me ustroivat, puskaite zaiavkata.
Pozdravi,
Veselin Paunov. --- On **Thu, 3/28/13, Емилия Машиах** ***<ctbloan@nacid.bg>*** wrote:

From: Емилия Машиах <ctbloan@nacid.bg>
Subject: otnosno zayavka v NACID-CNTB za statia
To: veskopaunov@yahoo.com
Date: Thursday, March 28, 2013, 4:31 AM

Уважаеми господин Паунов,
Исканата от Вас статия може да бъде доставена от чужбина. Цената на доставката е 8 евро= 19,56лв.
Можете да получите статията на посочен от Вас e-mail адрес или като хартиено копие след превеждане на посочената сума по банков път или на място в библиотеката. След получаване на статията при нас от чужбина, ще Ви изпратя банковите ни реквизити.
Ако условията Ви устройват, моля пишете ми на този e-mail адрес, за да пусна заявката.
Ако имате и други въпроси, не се безпокойте да ми пишете.
Приятен ден!
Емилия Машиах

27.03.2013 15:48 193.30.230.27
Моля приемете следното заявление за доставка на литература:
H. K. Kansal, Sehijpal Singh, Pradeep Kumar:
Numerical simulation of powder mixed electric discharge machining (PMEDM) using finite element method.
Mathematical and Computer Modelling 47(11-12): 1217-1237 (2008)
Място на търсене/доставка от *: 1. Библиотеки в чужбина;
Заявител *: Веселин Илиев Паунов
Организация *: Химикотехнологичен и металургичен университет
Адрес *: бул. Климент Охридски №8 София, 1756
E-mail *: veskopaunov@yahoo.com Начин на доставка *: По e-mail
Вид на доставката *: Копие Форма на плащане *: Банков път
****

Available online at www.sciencedirect.com
ScienceDirect
Mathematical and Computer Modelling 47 (2008) 1217–1237
MATHEMATICAL AND COMPUTER MODELLING
www.elsevier.com/locate/mcm

Numerical simulation of powder mixed electric discharge machining (PMEDM) using finite element method

H.K. Kansal[a,*], Sehijpal Singh[b], Pradeep Kumar[c]

[a] *Department of Mechanical Engineering, SLIET Longowal, Punjab, 148001, India*
[b] *Department of Mechanical and Production Engg, G.N.D.E.C. Ludhiana, Punjab, 147001, India*
[c] *Department of Mechanical and Industrial Engg, I.I.T. Roorkee, 247667, India*

Received 14 March 2006; received in revised form 22 February 2007; accepted 22 May 2007

Abstract

In the present paper, an axisymmetric two-dimensional model for powder mixed electric discharge machining (PMEDM) has been developed using the finite element method (FEM). The model utilizes the several important aspects such as temperature-sensitive material properties, shape and size of heat source (Gaussian heat distribution), percentage distribution of heat among tool, workpiece and dielectric fluid, pulse on/off time, material ejection efficiency and phase change (enthalpy) etc. to predict the thermal behaviour and material removal mechanism in PMEDM process. The developed model first calculates the temperature distribution in the workpiece material using ANSYS (version 5.4) software and then material removal rate (MRR) is estimated from the temperature profiles. The effect of various process parameters on temperature distributions along the radius and depth of the workpiece has been reported. Finally, the model has been validated by comparing the theoretical MRR with the experimental one obtained from a newly designed experimental setup developed in the laboratory.

Keywords: Powder mixed EDM; Temperature distributions; Finite element method; Material removal rate; Modeling; Simulation

1. Introduction

Electrical discharge machining (EDM) is one of most popular nonconventional machining processes used for creating complex shapes within the parts and assemblies in the manufacturing industry [1]. Its unique feature of using thermal energy to machine electrically conductive parts regardless of hardness has been its distinctive advantage. However, it suffers from few limitations such as low machining efficiency and poor surface finish. To overcome these limitations, a number of efforts have been made to develop such EDM systems that have capability of high material removal rate (MRR), high accuracy and precision without making any major alterations in its basic principle [2–5]. The techniques used in the past include (i) electrode rotating, (ii) electrode orbiting — planetary motion to tool or workpiece, (iii) applications of ultrasonic vibrations and (iv) suspension of foreign powders in the dielectric fluid. Among them, the mixing of a suitable material in powder form into the dielectric fluid is one of the latest advancement

* Corresponding author.
E-mail addresses: shaarut@yahoo.com (H.K. Kansal), sehijgnec@yahoo.co.in (S. Singh), kumarfme@iitr.ernet.in (P. Kumar).

0895-7177/$ - see front matter © 2007 Elsevier Ltd. All rights reserved.
doi:10.1016/j.mcm.2007.05.016

for improving the capabilities of EDM process [5–8]. This process is called powder mixed EDM (PMEDM). In this process, the electrically conductive powder particles are mixed in the dielectric fluid, which reduces its insulating strength and increases the spark gap distance between the tool and workpiece. The underlying idea is to spread the electric discharge uniformly in all directions. As a result; the process becomes more stable thereby improving material removal rate (MRR) and surface finish.

The machining mechanism of EDM is complex as it involves numerous phenomena like heat conduction and radiation, phase changes, electrical forces, bubble formation and collapse, rapid solidification. Further the suspension of powder particles into dielectric fluid makes it more complex and random. Several researchers have reported the effect of various powder particles in dielectric fluid of EDM [9–14]. However, the key issue of machining mechanism of PMEDM i.e. the action of powder suspended into the dielectric fluid is not clearly understood. A lot of work has been reported on the modeling of EDM [15–23]; however the role of powder suspended in the dielectric fluid of EDM has to date remained unexamined.

In the present paper, an effort has been made to study the effect of powder suspended in the dielectric fluid of EDM on process performance. A standard FEM package, ANSYS version 5.4 has been used to develop a numerical model of the PMEDM process [24]. The model considered the important aspects of the process such as temperature-sensitive material properties, type and nature of suspended powder, shape and size of heat source, percentage distribution of heat between tool, workpiece and dielectric fluid, pulse on/off time, and material ejection efficiency. It accounts for phase change by introducing the enthalpy concept. The primary innovation is the two-dimensional axisymmetric transient thermal analysis, including the study of the phase transformation due to highly localized heating and cooling effects of the discharge phenomenon on the workpiece surface. The effect of different PMEDM process parameters on temperature distribution has also been examined. The model has been validated using experimental values.

2. Numerical solution

In PMEDM, a series of rapid, repetitive and randomly distributed discrete electric sparks occur in the gap between tool and work electrodes for a cycle of few microseconds. Addition of powder particles into the dielectric fluid makes this process more complex and random. The following assumptions are made without sacrificing the basic features of the EDM model to make the problem mathematically feasible.

2.1. Assumptions

1. The model is developed for a single spark.
2. The thermal properties of workpiece material are considered as a function of temperature. It is assumed that due to thermal expansion, density and element shape are not affected [25].
3. To avoid the sharp changes in the heat capacity due to melting, enthalpy of the metal is considered as a function of temperature [26].
4. The heat source is assumed to have Gaussian distribution of heat flux on the surface of the workpiece [19,20].
5. The Material flushing efficiency is assumed to be 20% [19,20].
6. Conduction is considered as the mode of heat transfer to the electrodes.
7. The work domain considered is axisymmetric about r–z plane.
8. The composition of the material of workpiece is assumed to be homogeneous and isotropic [23].
9. Temperature analysis is considered to be of transient type [23,27].
10. The workpiece is free from any type of stress before PMEDM.

2.2. Thermal model

The discharge phenomenon in EDM can be modeled as the heating of the work electrode by the incident plasma channel. Fig. 1 shows the idealized case where workpiece is being heated by a Gaussian type of heat source. The mode of heat transfer in solid is conduction.

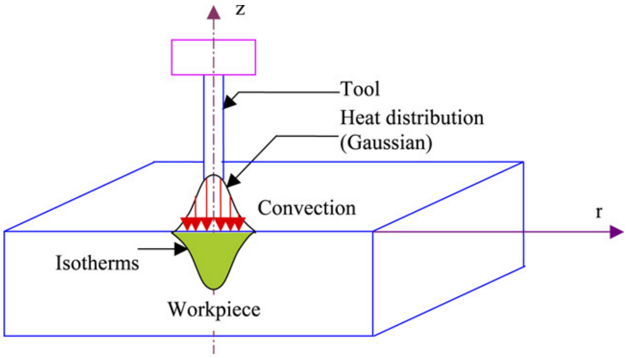

Fig. 1. Schematic sketch of Gaussian heat distribution in PMEDM.

2.2.1. *Governing equation*

The differential equation governing the heat conduction in an axisymmetric solid surface is given by [28]:

$$\rho C_P \frac{\partial T}{\partial t} = \left[\frac{1}{r}\frac{\partial}{\partial r}\left(Kr\frac{\partial T}{\partial r}\right) + \frac{\partial}{\partial z}\left(K\frac{\partial T}{\partial z}\right)\right] \tag{1}$$

where, ρ is the density, C_P is the specific heat and K is the thermal conductivity of the work material, T is the temperature, t is the time and r and z are coordinate axes shown in Fig. 1.

2.2.2. *Heat distribution*

For analytical tractability, many authors have used uniform disc heat source [15–18]. However, DiBitonto et al. [19–21] and Bhattacharya et al. [22] have shown that Gaussian heat distribution is more realistic than disc heat source. Moreover, the assumption of Gaussian distribution is well-accepted for modeling the heat input in EDM. Therefore, Gaussian heat distribution has been considered in the present work (Fig. 1).

2.2.3. *Boundary conditions*

The workpiece is symmetric about *z-axis*, so taking advantage of its symmetry; a small half-plane is cut from the workpiece (CDEF) with negligible thickness. The considered workpiece domain is shown in Fig. 2. In the domain, heat flux for a single spark is applied on the surface B_1 up to spark radius R using Gaussian distribution. On the remaining region on B_1 surface, the convection heat transfer takes place due to the cooling effect caused by the powder mixed dielectric fluid. As the boundaries B_2 and B_3 are very far from the spark radius and also the spark has been made to strike for a very little moment, no heat transfer conditions have been assumed for them. For B_4, which is the axis of symmetry, the heat flux has been taken as zero as there is no net heat gain or loss from this region.

In summary, the boundary conditions are given as follows:

1. *For boundary* B_1:
   Up to spark radius, R:
   $$K\frac{\partial T}{\partial z} = Q_W(r).$$
   Beyond spark radius, R:
   $$K\frac{\partial T}{\partial z} = h(T - T_0).$$
2. *For boundary* B_2, B_3, B_4:
   $$\frac{\partial T}{\partial n} = 0$$

where, h is the heat transfer coefficient between the workpiece surface and powder mixed dielectric, $Q_{W(r)}$ is the heat flux owing to the spark, T_0 is the initial temperature which is equal to room temperature and T is the temperature.

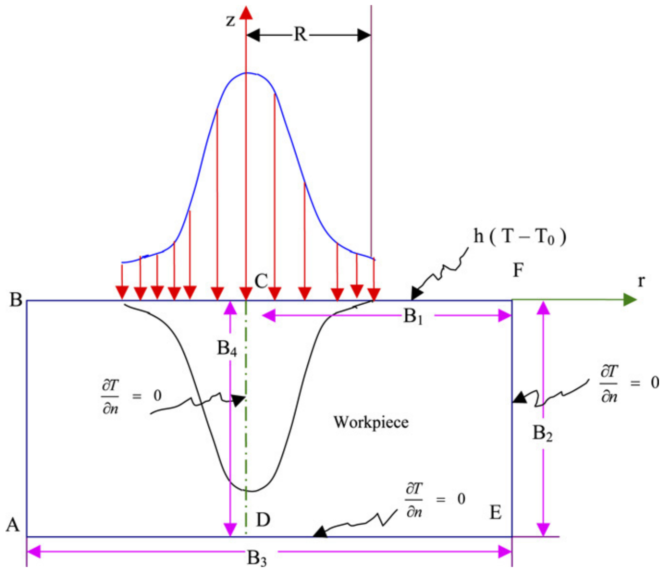

Fig. 2. Heat transfer model for PMEDM.

2.2.4. *Shape of the domain*

As the tool and the workpiece have been assumed to be thermally isotropic, therefore, the heat distribution would be Gaussian in nature on the surface of both workpiece and tool. Furthermore, the domain ∃, upon which the heat flux is incident is assumed to grow with time.

2.2.5. *Material properties*

PMEDM is a thermal process where huge thermal energy is generated. This causes instant rise in the workpiece temperature up to boiling point of the material and a subsequent decrease to room temperature. The abrupt change in the temperature severely affects the properties of the material. In this research work, the variations in the material properties with temperature are taken into account. The material of the workpiece considered in this study is high carbon high chrome (comparable to AISI D2) die steel. The chemical composition of work material and its various properties (mechanical and thermal) are mentioned in Table 1.

2.2.6. *Heat input to workpiece*

Earlier EDM models assumed that the total heat supplied on the surface is transferred to the workpiece and no heat is lost to the dielectric fluid and tool electrode [15–18,22,29]. However this assumption was not realistic. DiBitonto et al. [19] and Patel et al. [20] have assumed that a constant fraction of the total applied heat is lost to the electrodes. They predicted that about 8% of the total heat supplied is absorbed by anode; about 18% is absorbed by cathode and the rest is discharged to the dielectric fluid. Shanker et al. has calculated that 40%–45% of the heat input is absorbed by the workpiece [27]. However all the calculations have been made using water as the dielectric fluid and at different processing conditions.

As explained earlier, the powder particles suspended into the dielectric fluid increase the electrical conductivity of the dielectric fluid and help to spread the discharge uniformly in all directions. As a result, the fraction of the energy transferred to the workpiece (R_W) may be larger than that of EDM. However, there is no theoretical and experimental method to calculate the value of R_W during PMEDM. In the present model; it has been assumed that 9% of the total heat is lost to the workpiece.

2.2.7. *Material flushing efficiency*

Most of the existing modeling studies on EDM have assumed that the material flushing efficiency (MFE) is 100% i.e. all the molten metal is removed from the crater produced on the surface. However, experimental results have shown that not all the molten metal is ejected [19,20]. In fact, only 10%–30% is actually ejected. As a result, deviations of experimental results from theoretical results are often observed. In the present work, the MFE is assumed to be 20%.

Table 1
Chemical composition mechanical and thermal properties of AISID2 die steel

Chemical composition							
Element	C	Si	Mn	W	V	Mo	Cr
%	1.52	0.3	0.3	0.5	0.10	0.8	12

Mechanical properties	
Density, ρ	7700 kg/m^3
Young's modulus, E	208 GN/m^2
Melting temperature, T_m	1984 K
Reference temperature, T_o	298 K
Poisson's ratio, υ	0.3
Max. yield strength, S_{yield}	3300 MPa
Latent heat melting, L_m	2746 kJ/kg
Latent heat for evaporation, L_{ev}	1586 kJ/kg

Thermal properties			
Temperature (K)	Th conductivity (W/m °C)	Coefficient of thermal expansion (/°C)	Specific heat (J/kg/K)
298	29.0	5.71×10^{-6}	412.21
673	29.5	6.90×10^{-6}	418.36
1100	30.7	10.20×10^{-6}	421.83
1990	32.3	12.00×10^{-6}	431.00

2.2.8. *Spark radius*

It is well-established that the size of plasma channel is not a constant but it grows with time [19]. Its growth depends upon various factors such as electrode material, electrode arrangement and polarity [30]. Some researchers have tried theoretically and experimentally to determine the spark radius (R) in EDM [15,31]. DiBitonto et al. have calculated the radius of the discharge channel mathematically in the form of integral equation for rectangular pulses [19]. Erden further integrated this equation and found that the radius of discharge channel $R(t)$ is dependent on the discharge power and time according to relationship [32]:

$$R(t) = ZP^m t^n \tag{2}$$

where, P is the discharge power, t is time and Z, m and n are empirical constants, with Z being a function of the discharge length. Further these constants have been defined in terms of experimental coefficients L, M and N as:

$$Z = \frac{L}{lm + 0.5N}; \quad m = M + 0.5N \text{ and } n = N \tag{3}$$

where, l is the discharge length.

Further, to predict the two-dimensional shape of the arc of plasma channel, Ayyaswamy et al. [33] and Cohen et al. employed a "tanh" (hyperbolic tangent) model [34]. Shanker et al. have predicted the arc radii at different cross-sections of the plasma channel [27].

In PMEDM, the powder mixed into the dielectric fluid helps the discharge to spread uniformly in all directions, resulting in an enlarged and widened discharge channel. Experimental studies on PMEDM revealed that the spark gap is enlarged and widened by a factor of 2 or 3 of conventional EDM [35–39]. Further, Zhao et al. have shown that addition of powder into dielectric fluid of EDM helps to produce small and shallow craters on the surface of workpiece [5]. However, a reliable and realistic method of determining the spark radius by either theoretical/experimental analysis has not been reported. In this work, the radius of the spark for PMEDM is taken to be 30%–50% larger than that found by Shankar et al. [27].

2.2.9. *Latent heat*

In EDM, the electrode (tool) and workpiece are repeatedly heated above the melting points and are allowed to cool in the dielectric fluid. This causes a change in the phase of the material. The phase change requires an energy input

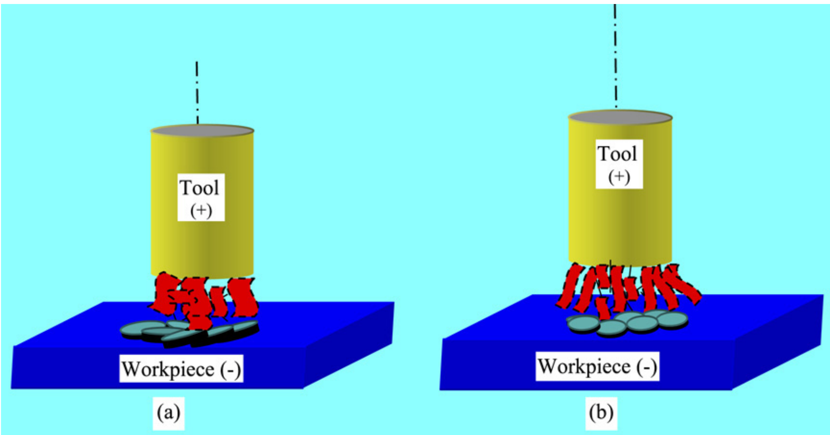

Fig. 3. Spark frequency in: (a) EDM, (b) PMEDM.

equivalent to the latent heat. In the present work, the effect of latent heat is considered to make the model more realistic and reliable. Therefore, specific heat for melting and evaporation are modified as given below by incorporating the latent heat of melting and evaporation [22].

$$C_m = C_P + \frac{L_m}{2\Delta T} \quad \text{for } T_m - \Delta T \leq T \leq T_m + \Delta T \tag{4}$$

and

$$C_{\mathrm{ev}} = C_m + \frac{L_{\mathrm{ev}}}{2\Delta T} \quad \text{for } T_{\mathrm{ev}} - \Delta T \leq T \leq T_{\mathrm{ev}} + \Delta T \tag{5}$$

where, C_P is specific heat of workpiece, C_m is specific heat in melting state, C_{ev} is specific heat in evaporation state, L_m is latent heat due to melting and L_{ev} is latent heat due to evaporation.

2.2.10. Spark frequency and breakdown voltage

Spark frequency is a measure of the number of times the discharge strikes against the surface of the workpiece. In the case of PMEDM, the powder suspended in the dielectric fluid gets energized and behaves in a zigzag fashion. The suspended powder particles enlarge and widen the spark gap between both the electrodes and change the ionization–deionization characteristics of the dielectric fluid as shown in Fig. 3. With increase in the gap distance, an appropriate reduction in the breakdown voltage (electrostatic capacity) occurs, which results in more discharges per unit time (spark frequency). Experimentally, it has been found that in PMEDM, the discharge frequency is about 2–3 times higher than that in EDM, whereas the breakdown voltage is about 20%–30% lower than that for EDM process [5, 35,37]. The increased spark frequency and reduced voltage produce more small and shallow craters i.e. more even machining is achieved. The reason being that energy available for material removal during a given period is shared by large number of powder particles and the magnitude of the impact force, which acts on the workpiece surface, is smaller than the conventional EDM. Fig. 3(a) shows that the size of the crater produced by EDM is big and its surface is rough. However, in PMEDM, the craters are shallow and smaller in size (see Fig. 3(b)).

To take into account the effect of powder on spark frequency and breakdown voltage, a new parameter, K_n, is introduced into the heat flux equation (the derivation of which is presented in Section 2.2.11). The value of K_n, depends upon the type of powder, powder properties such as shape, size, concentration etc. In the present work, the parameter K_n, is estimated empirically by conducting experiments with graphite powder mixed dielectric fluid and without powder (conventional EDM) under the same machining conditions.

2.2.11. Heat flux

Most researchers have considered the hemi-spherical disc heat source for thermal modeling in EDM. However, this approximation is neither realistic nor reliable. It has been reported in [19–22] that the isothermal curves obtained for EDM thermal model can be accurately approximated by Gaussian distribution. Yadava et al. have reported a heat flux

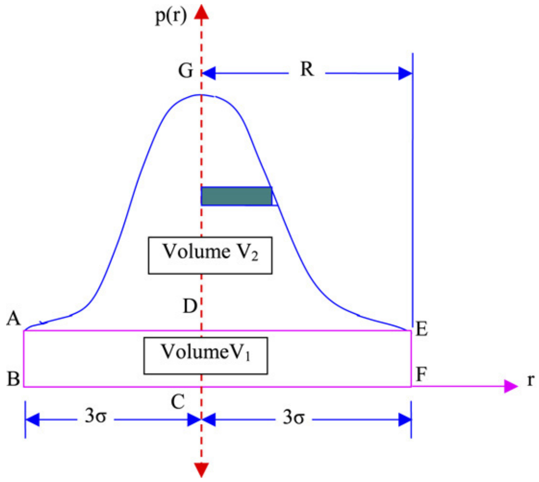

Fig. 4. Gaussian distribution.

equation for EDM considering the Gaussian distribution [23]. To consider the effect of suspended powder particles into dielectric fluid on PMEDM, the same has been modified as given below:

The probability density function (pdf) of Gaussian distribution for a random variable r is shown in Fig. 4 and is given by the relation [39]:

$$p(r) = \frac{1}{\sqrt{2\pi}\sigma} e^{-\frac{r^2}{2\sigma^2}} \tag{6}$$

where, $\frac{1}{\sqrt{2\pi}\sigma}$ is the peak value of the distribution and σ is the standard deviation.

Since the Gaussian curve does not mathematically become zero until infinity, it becomes necessary to select some finite large value of its argument to represent the bottom of the crater. Usually six times of σ (-3σ to $+3\sigma$) is taken for dropping the response to 0.25% of its initial value i.e. 99.75% of the values lies between $r = \mu - 3\sigma$ and $r = \mu + 3\sigma$ (see Fig. 4). The profile of a three-dimensional crater can be obtained by rotating the Gaussian curve around the vertical axis.

Therefore, $R = 3\sigma$. Substituting the value of σ into Eq. (6)

$$p(r) = \frac{3}{\sqrt{2\pi} R} e^{-4.5\frac{r^2}{R^2}}. \tag{7}$$

In PMEDM, $p(r)$ is the intensity of heat imparted to the workpiece surface, which is denoted by Q_W and is a function of r.

$$\text{At } r = 0, \quad p(r) = Q_0;$$

where Q_0 is the maximum intensity of heat applied at the center of the workpiece. Therefore, the heat flux of the system (Eq. (7)) is given by

$$Q_W(r) = Q_0 e^{-4.5\frac{r^2}{R^2}}. \tag{8}$$

Thus the energy incident on the workpiece is

$$\begin{aligned}\oint Q_w(r)\mathrm{d}A &= \int_0^R Q_w(r) 2\pi r \mathrm{d}r \\ &= \int_0^R Q_0 e^{-4.5\frac{r^2}{R^2}} 2\pi r \mathrm{d}r\end{aligned}$$

$$= -\frac{\pi R^2}{4.5} Q_0 e^{-4.5\frac{r^2}{R^2}}\Big|_0^R$$
$$= \frac{\pi R^2 Q_0}{4.5}(1 - e^{-4.5})$$
$$= 0.2191\pi Q_0 R^2. \tag{9}$$

The rate of energy incident on the workpiece is equal to the rate of energy supplied which is

$$R_W V_b I K_n \tag{10}$$

where, R_W is the fraction of heat input to the workpiece, V_b is the breakdown voltage, I is the current and K_n is new parameter introduced to take into account the effect of suspended powder particles on the spark frequency and breakdown voltage. The value of K_n depends upon the type of powder, powder properties such as shape, size, concentration etc.

Therefore,

$$R_W V_b I K_n = 0.2191\pi Q_0 R^2$$

or

$$Q_0 = \frac{4.57 K_n V_b I R_W}{\pi R^2}. \tag{11}$$

Upon substitution of Eq. (11) into (8),

$$Q_W(r) = \frac{4.57 K_n V_b I R_W}{\pi R^2} e^{-4.5(\frac{r}{R})^2}. \tag{12}$$

2.3. Applications of FEM in thermal modeling of PMEDM

Finite Element Method (FEM) is a powerful tool for obtaining the approximate solution of real engineering problems [40]. It can handle wide range of engineering problems of complex geometry, materials, loading and boundary conditions. It uses discretization of a continuum domain into finite numbers of parts called elements and seeks solution at discrete points of the domain (nodes) using certain interpolation functions to approximate the primary variables over various elements of the domain.

For PMEDM analysis, the heat conduction Eq. (1) is required to be converted into FEM form and can be written in differential form as:

$$\rho C_P \left(\frac{\partial T}{\partial t}\right) + \{L\}^T \{Q_W\} = 0 \tag{13}$$

where, ρ is density, C_P is specific heat, T is temperature and t is time and

$$\{L\} = \begin{Bmatrix} \dfrac{\partial}{\partial r} \\ \dfrac{1}{r}\dfrac{\partial}{\partial \theta} \\ \dfrac{\partial}{\partial Z} \end{Bmatrix} = \text{Vector operator}, \qquad \{Q_W\} = \begin{Bmatrix} Q_r \\ Q_\theta \\ Q_Z \end{Bmatrix} = \text{Heat flux vector}.$$

For simplified analysis, the problem is made axisymmetric and the final geometry is reduced to a two-dimensional domain. Therefore, the vector operator and heat flux vector are reduced to two-dimensional forms as given below:

$$\{L\} = \begin{Bmatrix} \dfrac{\partial}{\partial r} \\ \dfrac{\partial}{\partial Z} \end{Bmatrix}, \qquad \{Q_W\} = \begin{Bmatrix} Q_r \\ Q_Z \end{Bmatrix}.$$

The variable T is allowed to vary in both space and time. This dependency is separated as:

$$T = \{N\}^T \{T_e\} \tag{14}$$

where, $\{N\}$ = Element shape function vector, $\{T_e\}$ = Element's Nodal temperature vector

Further, the time derivatives of Eq. (14) may be written as:

$$\frac{\partial T}{\partial t} = \dot{T} = \{N\}^T \left\{\dot{T}_e\right\} = 0. \tag{15}$$

After combining $\{L\}$ with T, the expression for temperature (T) can be written as:

$$\{L\} T = [B] \{T_e\} \tag{16}$$

where, $[B]$ = Shape function derivative matrix evaluated at the integration points

$$= \{L\} \{N\}^T .$$

Further, let δT be the small change in the temperature at the node. The δT can be written in a similar form to T

$$\delta T = \delta T_e^T \{N\}. \tag{17}$$

Now, the variational statement becomes

$$\begin{aligned} &\int_V \rho C_P \{\delta T_e\}^T \{N\}\{N\}^T \{\dot{T}_e\} \mathrm{d}V + \int_V \{\delta T_e\}^T [B]^T [K][B]\{T_e\} \mathrm{d}V \\ &\quad = \int_{\exists_b} \{\delta T_e\}^T \{N\} Q_W \mathrm{d}\exists_b + \int_{\exists_{b_1}} \{\delta T_e\}^T \{N\} h(T - \{N\}^T \{T_e\}) \mathrm{d}\exists_{b_1} \end{aligned} \tag{18}$$

where, $[K]$ = conductivity matrix, ρ = density, C_P = specific heat, V = volume, T = temperature, h = coefficient of heat transfer, $\exists_b$ is the domain of boundary element $\left\{\dot{T}_e\right\}$ and $\{\delta T_e\}$ are nodal quantities which do not vary.

In Eq. (18), all the quantities are seen to be premultiplied by the arbitrary vector $\{\delta T_e\}^T$, this term can be dropped from the resulting equation. Thus the Eq. (18) reduces to:

$$\begin{aligned} &\rho \int_V C_P \{N\}\{N\}^T \{\dot{T}_e\} \mathrm{d}V + \int_V [B]^T [K][B]\{T_e\} \mathrm{d}V \\ &\quad = \int_{\exists_b} \{N\} Q_W \mathrm{d}\exists_b + \int_{\exists_{b_1}} \{N\} h(T - \{N\}^T \{T_e\}) \mathrm{d}\exists_{b_1}. \end{aligned} \tag{19}$$

The Eq. (19) can be written in final assembled finite element form as:

$$[C_{Pe}] \left\{\dot{T}_e\right\} + ([K_e^d]) \{T_e\} = \{Q_e\} + \left\{Q_e^c\right\} \tag{20}$$

where,

$$[C_{Pe}] = \rho \int_V C_P \{N\}\{N\}^T \mathrm{d}V = \text{Elemental capacitance (specific heat) matrix}$$

$$[K_e^d] = \int_V [B]^T [K][B] \mathrm{d}V = \text{Element diffusion conductivity matrix}$$

$$\{Q_e\} = \int_{\exists_b} \{N\} Q_W \mathrm{d}\exists_b = \text{Element mass flux vector}$$

$$\left\{Q_e^c\right\} = \int_{\exists_{b1}} T h \{N\} \mathrm{d}\exists_b = \text{Element convection surface heat flow vector.}$$

In differential form, the Eq. (20) can be written as:

$$[C_G]\{\dot{T}_G\} + [K_G]\{T_G\} = \{Q_G\} \tag{21}$$

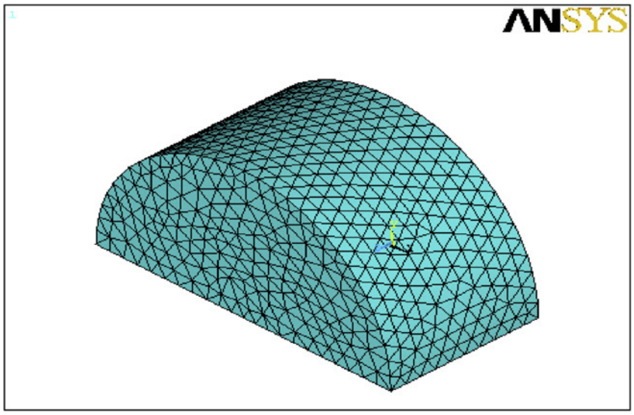

Fig. 5. Three-dimensional view of the meshed model.

where, $[C_G]$ = Global capacitance (specific heat) matrix, $[K_G]$ = Global conductivity matrix, $\{Q_G\}$ = Global heat flux vector, $\{T_G\}$ = Global temperature vector, and $\{\dot{T}_G\}$ = Time derivative of $\{T_G\}$.

This equation is simply the matrix equivalent of Eq. (1). The standard solver of the ANSYS program has been used to solve this system equation.

2.4. Modeling procedure using ANSYS

PMEDM is a complicated thermal process that involves complex interaction of different physical phenomena. FEM makes it possible to simulate the workpiece temperature and stress distributions. To develop the FEM based PMEDM model, a powerful software is required which can consider all complicated aspects of the process. ANSYS is one such powerful tool that can be used in FEM analysis of the different models [24]. Any complicated geometry can be analyzed easily using ANSYS. It has many finite element analysis capabilities, ranging from a simple, linear, static analysis to a complex, nonlinear, transient dynamic analysis in the fields such as structural mechanics, thermal systems, fluid mechanics, and electromagnetics. In the present research work, the modeling and simulation of results for PMEDM have been performed using ANSYS software [24]. The work geometry has been created in ANSYS using appropriate boundary conditions. The different kinds of loads are applied on the work domain. Meshing of the workpiece domain is done using mapped meshing technique. This technique has a pattern of either only quadrilaterals or only triangular elements.

The following steps describe the detailed procedure used for thermal modeling of PMEDM using ANSYS:

Step 1: Objective: The objective of this analysis is to find out the temperature distribution on the workpiece processed by PMEDM.
Step 2: Units: S.I.
Step 3: Product selection: ANSYS/Multiphysics-1
Step 4: Analysis method: Thermal, h method
Step 5: Type of analysis: Transient
Step 6: Problem domain: In this step, the geometry of the problem is created using ANSYS. Three-dimensional workpiece geometry is created. However, the domain is axisymmetric about z-axis, therefore, taking the advantage of its axisymmetry; the final geometry is reduced to a two-dimensional diagram. The dimensions of the workpiece domain are 0.625 mm × 0.625 mm. The meshed three-dimensional and two-dimensional models are shown in Figs. 5 and 6 respectively.
Step 7: Choice of element: Two-dimensional, 4 Noded Quadrilateral Element (thermal solid plane 55) with 20 μm size.

2.5. Determination of material removal rate (MRR) from FEM

The temperature profile obtained from FEM analysis is used to calculate the amount of material removed from the surface of the workpiece that is exposed to the heat flux. A failure criterion is applied which correlates the temperature with the possibility of failure, to predict which part of the material is failing due to the heat flux given

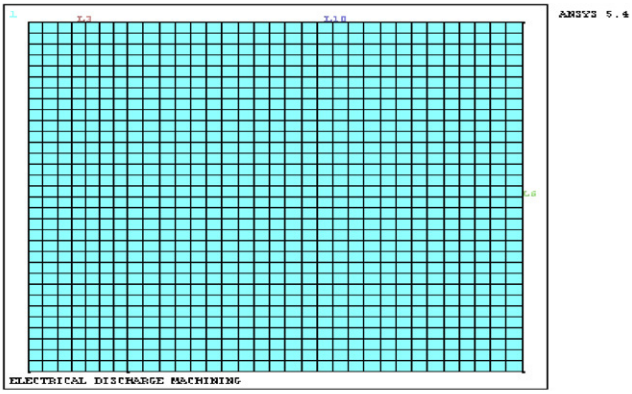

Fig. 6. Two-dimensional view of the meshed model.

Table 2
Process parameters for PMEDM

Parameter	Value
Voltage, V	30 V
Current, I	3.2–12 A with three levels (3.2, 6.5 and 12 A)
Heat input to workpiece, R_W	9%–20% with four levels (5%, 9%, 15% and 20%)
Radius of spark, R	120 μm
Pulse duration, T_{on}	100–300 μs with three levels (100, 200 and 300 μs)
Pulse off time, T_{off}	100–300 μs with four levels (50, 100, 200 and 300 μs)
Type of flushing	Side nozzle flushing
Polarity	+ve
Powder type and size	Graphite, 30 μm in average
Frequency constant, K_n	2.4
Powder concentration	2 g/l
Electrode lift time	0.2 s
Tool electrode diameter	15 mm

on the workpiece surface. According to the failure criterion a region in the temperature profile is identified, where the temperature is greater than the melting temperature of the workpiece material (1984 K). The material from that zone where temperature exceeds the melting temperature of the workpiece is assumed to be eroded due to spark.

3. Analysis and discussion of results

To obtain the results from the developed FEM model for PMEDM, AISID2 die steel is considered as the workpiece material and copper as a tool material. The AISID2 die steel is one of the most common tool steel used for EDM applications and is machined best by copper electrode. The chemical composition, thermal and mechanical properties of AISID2 is mentioned in Table 1. The model is developed using the process parameters given in Table 2. Later, the developed FEM model is validated by comparing the predicted theoretical results with the experimental data.

The predicted temperature isotherms for a single spark of PMEDM and EDM are shown in Figs. 7 and 8 respectively. As expected, the predicted maximum temperature is located at the center, where intensity of heat flux applied is maximum. The magnitude of temperature decreases as we move away from the centerline.

The study of Figs. 7 and 8 reveals the following four distinct regions:

(a) boiling region (red colour),
(b) liquid region (up to light green colour),
(c) HAZ (up to light blue colour) and
(d) Solid metal (blue colour).

It can be observed that the heat is spread to a longer distance in the workpiece machined by PMEDM as compared to EDM under the same machining conditions. The size of the crater produced by PMEDM is longer in radial direction

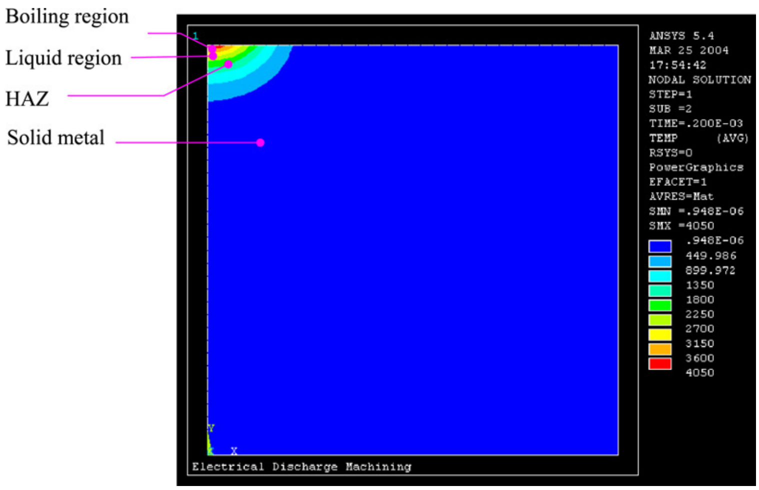

Fig. 7. Temperature isotherms due to single spark of PMEDM process for the half-section of workpiece. (For interpretation of the references to colour in this figure legend, the reader is referred to the web version of this article.)

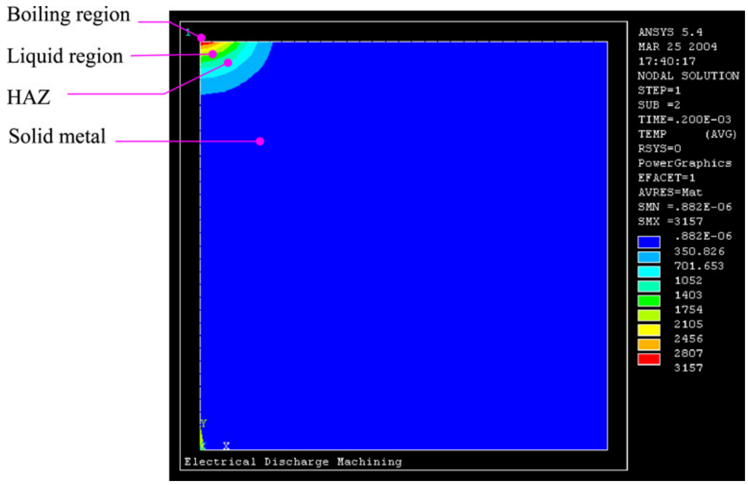

Fig. 8. Temperature isotherms due to single spark of EDM process for the half-section of workpiece. (For interpretation of the references to colour in this figure legend, the reader is referred to the web version of this article.)

while the depth of crater is not changed appreciably in comparison to EDM. However, due to increase in discharge frequency, the overlapping of craters takes place and craters look smaller in size. Therefore, it can be concluded that for the same process parameters, smaller and shallower craters are produced by using PMEDM than by using EDM. This verifies the proposed machining mechanism of PMEDM i.e. the powder suspended into the dielectric fluid enlarges and widens the discharge channel which help to spread the heat uniformly in all directions, thereby improving the surface finish at relatively high machining rates.

Further, the distribution of temperature and its level in the workpiece material depends upon various process parameters such as peak current, pulse duration, pulse off time, amount of energy input to workpiece, phase change and type of powder suspended into the dielectric fluid of EDM. The effect of variation of these process parameters on the temperature isotherms is explained below.

3.1. Effect of current

The variation of the surface temperature with distance (along radius and depth of workpiece) has been plotted for three different values of peak current (3.2, 6.5 and 12 A) and is shown in Figs. 9 and 10. From these figures, it can be

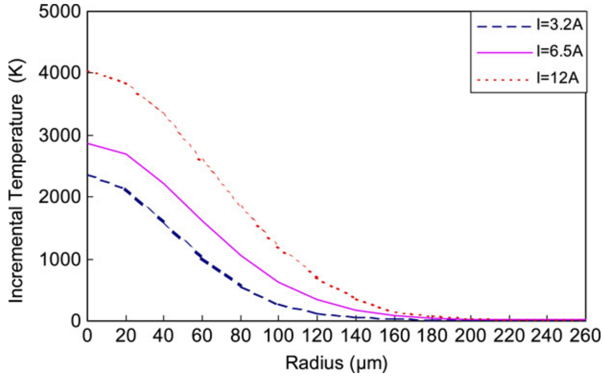

Fig. 9. The effect of peak current on the temperature distribution along the radial direction from the centerline for PMEDM at $T_{on} = 100$ μs, $T_{off} = 100$ μs, $V = 30$ V, $R_W = 9\%$, and with graphite powder.

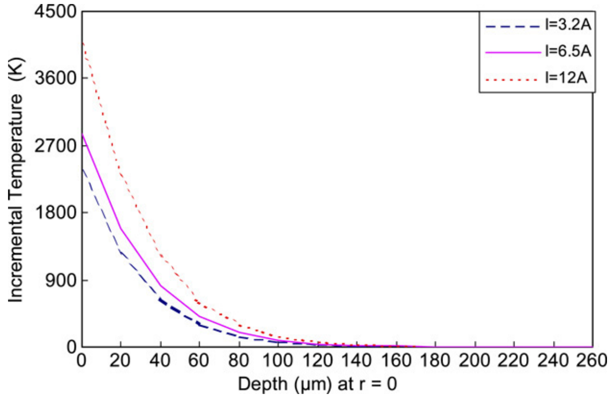

Fig. 10. The effect of peak current on the temperature distribution along depth of workpiece at the centerline for PMEDM at $T_{on} = 100$ μs, $T_{off} = 100$ μs, $V = 30$ V, $R_W = 9\%$, and with graphite powder.

observed that the top surface temperature goes on increasing with increase in current. This is because, the current is a function of the heat energy transferred to the workpiece. The larger the current, the greater the heat energy generated and transferred to the workpiece. Further, from Fig. 9, it can be seen that the distribution of temperature follows the shape of Gaussian curve (bell shape). As expected, farther the distance from the workpiece surface, lower the temperature. The considerable temperature gradient along the radial direction can be seen up to the radius of 140 μm.

The temperature variation along the depth of the workpiece is shown in Fig. 10. It can be observed that the temperature is maximum at the top surface and decreases as we proceed downward. The workpiece material at the depth of 50 μm looks very sensitive to be the house of residual stresses, because, in this region, the variation in temperature is very sharp. No variation in temperature is observed after a depth of 100 μm. Hence it can be concluded that the material removal rate is more along the radial direction than along the depth resulting in shallow craters.

3.2. Effect of pulse duration

The effect of variation in pulse duration on surface temperature distribution in PMEDM along radius and depth are plotted in Figs. 11 and 12 respectively. From the trend of variation in surface temperature along the radius of the workpiece, it can be observed that with increase in pulse duration, the surface temperature also increases. It is obvious because, if heat is supplied for a longer time period, the temperature will be high. Further, near the point of spark, the temperature is very high. It decreases slowly as we move away from the workpiece. It could be seen that the temperature variation is slow up to the radius of about 60 μm. Beyond 60 μm, the rate of decrement is high. The reason being that as the heat flux is given for a longer period on workpiece surface, the temperature near the center will be high, but after that uniform heat dissipation occurs as the convection coefficient for the dielectric fluid is the same.

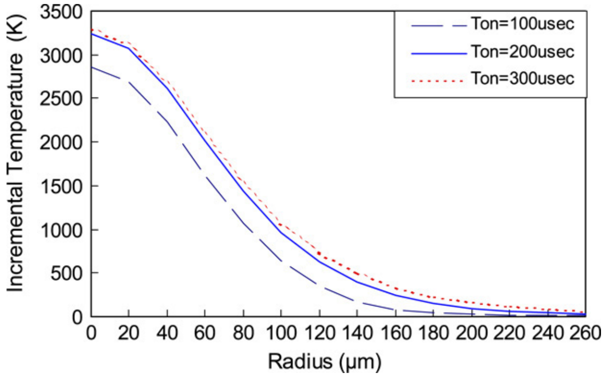

Fig. 11. The effect of pulse duration on the temperature distribution along radius of workpiece from the centerline for PMEDM at $I = 6.5$ A, $T_{\mathrm{off}} = 100$ μs, $V = 30$ V, $R_W = 9\%$, and with graphite powder.

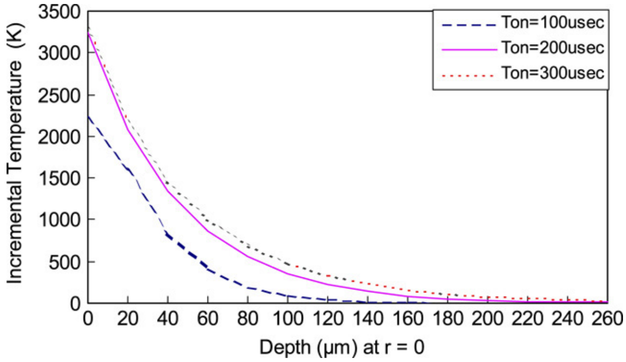

Fig. 12. The effect of pulse duration on the temperature distribution along depth of workpiece from the centerline for PMEDM at $I = 6.5$ A, $T_{\mathrm{off}} = 100$ μs, $V = 30$ V, $R_W = 9\%$, and with graphite powder.

Fig. 12 reveals that the temperature gradient is steeper than that along the radius. As we move deeper, the gradient for the longer pulse duration is small as compared to the gradient for the short pulse duration. This may be attributed to the shorter time for heat dissipation which is less for each duty cycle for longer pulse duration.

3.3. Effect of pulse off time

Figs. 13 and 14 show the effect of variation of pulse off time on the temperature distribution in workpiece material in PMEDM. The pulse off time is the time during which no energy is applied to the workpiece surface. The effect of pulse off time is studied by keeping the pulse duration constant. It is clear from the curves that the top surface temperature of the workpiece increases as the pulse off time decreases. This may be because, for short pulse off time, the time available for the application of heat energy on the workpiece surface will be long. Therefore, the material will be eroded at faster rate. However, the appropriate selection of pulse off time is very important for stable machining; too short a pulse interval will result in arcing while too long an interval results in long machining times.

Further, from Fig. 14, it can be seen that the trend of distribution of temperature along the radial direction is almost same for all the pulse off times. Very little difference is observed in temperature variation for 100 and 200 μs pulse off times. Similar trend of temperature distribution has been obtained along the depth of the workpiece for different pulse off values.

3.4. Effect of heat input to workpiece

As stated earlier, the heat input is the amount of heat energy transferred to the workpiece during machining. The effect of variation of heat input to workpiece along the radius and depth are shown in Figs. 15 and 16 respectively. From these figures, it can be observed that high surface temperature is attained at high value of energy partition.

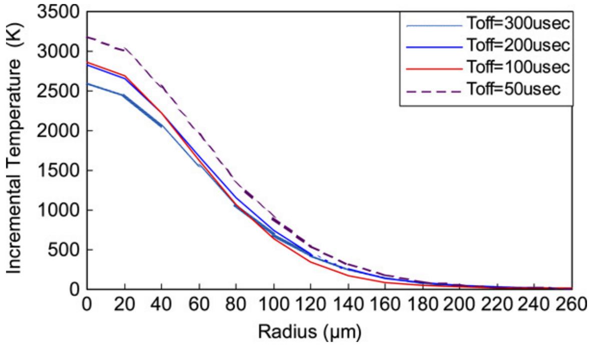

Fig. 13. The effect of pulse off time on temperature distribution along radius of workpiece from the centerline for PMEDM at $I = 6.5$ A, $T_{on} = 100$ μs, $V = 30$ V, $R_W = 9\%$, and with graphite powder.

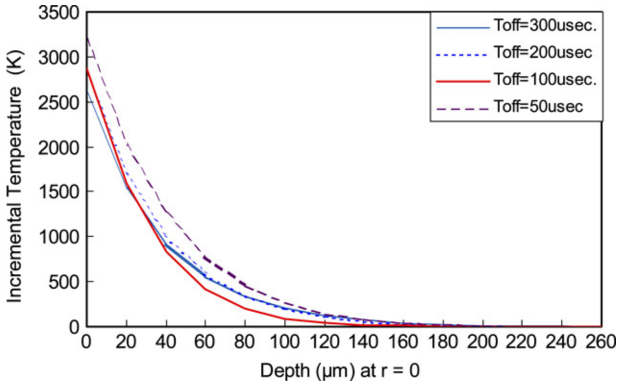

Fig. 14. The effect of pulse off time on temperature distribution along depth of workpiece from centerline for PMEDM at $I = 6.5$ A, $T_{on} = 100$ μs, $V = 30$ V, $R_W = 9\%$, and with graphite powder.

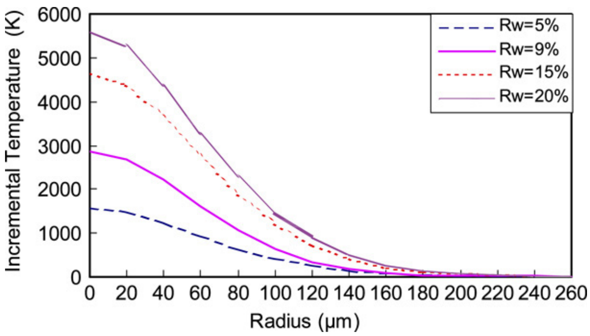

Fig. 15. The effect of heat input to workpiece on temperature distribution along radius at centerline of workpiece for PMEDM at $I = 6.5$ A, $T_{on} = 100$ μs, $T_{off} = 100$ μs, $V = 30$ V, and with graphite powder.

This is obvious because more amount of heat is transferred to the workpiece as large amount of heat is supplied to the workpiece. Another observation that can be drawn from these figures is that with 9% of heat input to workpiece, nearly 3000 K temperature is attained while, with 20% heat input, the top surface temperature is nearly 6000 K. In the former case, surface temperature is sufficient for its proper and controlled machining as melting temperature of AISID2 is below 3000 K i.e. 1984 K while in the latter, huge amount of heat is generated which makes it very difficult to control the precise and accurate machining of the workpiece. The PMEDM machined workpieces have very smooth and gloss surface texture [35]. This would be possible only if controlled and precise machining occurs there. Therefore it can be concluded that about 9% of heat energy partitioned to the workpiece is the sufficient amount of energy to produce the smooth craters. Further, the trend of variation in temperature is same for all the heat inputs to the workpiece.

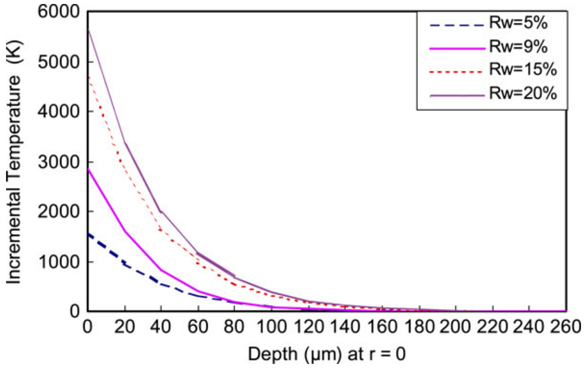

Fig. 16. The effect of heat input to workpiece on temperature distribution along depth at centerline of workpiece for PMEDM at $I = 6.5$ A, $T_{\text{on}} = 100$ μs, $T_{\text{off}} = 100$ μs, $V = 30$ V, and with graphite powder.

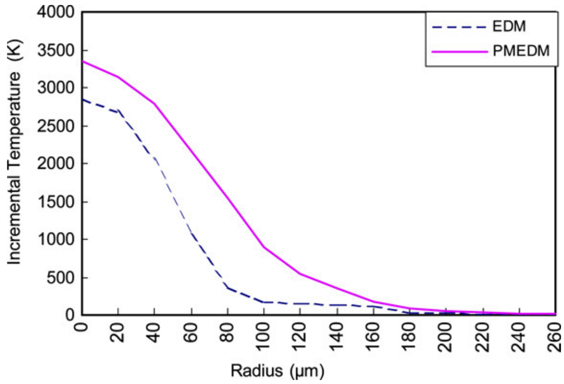

Fig. 17. The effect of phase change on temperature distribution along radius of workpiece at $I = 6.5$ A, $T_{\text{on}} = 100$ μs, $T_{\text{off}} = 100$ μs, $V = 30$ V, $R_W = 9\%$, and with graphite powder.

The comparison of temperature distributions along radius and depth of workpiece shows that the temperature gradient is high along the radius as compared to depth. The room temperature has been attained at a radius of about 140 μm as shown in Fig. 15 while the same is attained at 100 μm distance along the depth (see Fig. 16). This confirms that the shape of craters in PMEDM is elongated along the radius than at the depth i.e. bell shape craters are produced.

3.5. Effect of phase change

EDM is the thermal process in which enormous amount of heat is generated. Due to generation of huge amount of heat energy on the workpiece surface, the change in phase of the material is expected. Figs. 17 and 18 depict the effect of phase change on temperature distribution along radius and depth of workpiece. It can be observed that the top surface temperature is high when the effect of phase change is not considered. The reason behind it is that no heat energy is used to convert the state of material from solid to liquid and then to vapour. However, this does not happen in actual practice. Some part of the incident heat energy is always utilized for changing the state of the material. Further, temperature gradient is higher along the radius as compared to gradient along the depth of the workpiece when the effect of phase change is considered.

4. Model validation

To validate the proposed model, few PMEDM experiments were conducted under the same machining conditions at which simulation results are obtained. The machining conditions are given in Table 2. The experiments are performed on a newly designed experimental setup developed in the laboratory. The theoretical MRR values calculated from the temperature distributions were compared with the corresponding experimental MRR values. The experimental details follow:

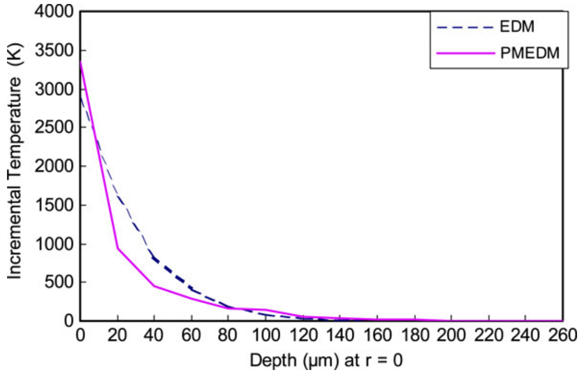

Fig. 18. The effect of phase change on temperature distribution along depth of workpiece at $r = 100\ \mu\text{m}$ at $I = 6.5$ A, $T_{\text{on}} = 100\ \mu\text{s}$, $T_{\text{off}} = 100\ \mu\text{s}$, $V = 30$ V, $R_W = 9\%$, and with graphite powder.

4.1. Experimental details

Experiments were conducted on a Mini G-30 die sinking EDM machine manufactured by ToolCraft India Ltd. Bangalore India. It is energized by A 15 type, 25-Ampere working current pulse generator and a controller to produce rectangular shaped current pulses. The current dielectric circulation system of G-30 EDM machine needs about 60 l of dielectric fluid (kerosene) in circulation. The powder could not be mixed with the circulating fluid because it would then be difficult to regulate the concentration of powder in the dielectric. Moreover, the system filter is liable to choke due to the presence of powder particles and debris. To overcome these problems, a new experimental setup for PMEDM was designed and developed in the laboratory. The schematic of kinematic configuration of the PMEDM set-up is shown in Fig. 19(a) and is photographed as shown in Fig. 19(b).

The new PMEDM system was designed for 7 l of dielectric fluid for experimentation. It consists of a transparent bath-like container, called machining tank in which the machining is performed. It contains a fixture assembly for holding the workpiece. The machining tank is filled up with dielectric fluid (kerosene oil). To avoid particle settling, a stirring system is incorporated. A small dielectric circulation pump is installed there for proper circulation of the powder mixed dielectric fluid into the discharge gap (power rating is 0.3H.P, flow rate 2 l/min and diameter of ejector nozzle is 4 mm). The pump and the stirrer are placed in the same tank in which machining is performed. The distance between powder mixed dielectric suction point and nozzle outlet is made short as possible (10 inches) in order to ensure the complete suspension of powder in the discharge gap. Magnetic forces are used to separate the debris from the dielectric fluid. For this purpose, two permanent magnets are placed at the bottom of machining tank. The experimental setup is demonstrated by the photograph shown in Fig. 19(b).

4.2. Workpiece and tool material

AISID2 die steel in fully annealed condition is selected as the workpiece material. The average hardness of the material was found to be 59HRC. Copper electrode with diameter 15 mm has been selected as the tool. The dimensions of workpiece are 100 mm × 50 mm × 10 mm. The machining is performed in commercially available kerosene oil after addition of graphite powder with average particle size 30 μm.

4.3. Validation

Fig. 20 presents the variation of MRR with pulse duration for EDM and PMEDM both theoretically and experimentally. A good correlation (coefficient of correlation = 0.91) between the calculated and predicted MRR is found. This proves the validity of the present model. The values of MRR obtained for PMEDM are always higher than the conventional EDM (both theoretically and experimentally). This is attributed to the powder suspension in the dielectric fluid of EDM that facilitates the uniform distribution of heat energy in all directions of the plasma channel. This produces relatively high machining rates.

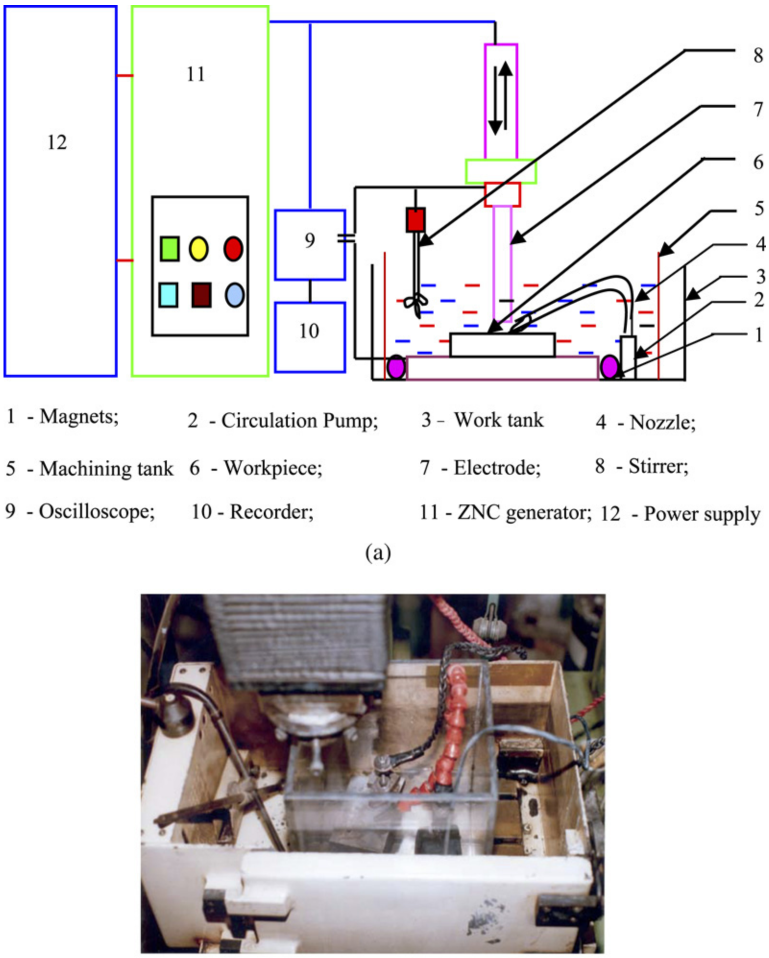

Fig. 19. (a) Schematic diagram of experimental setup and (b) real photograph of experimental setup for PMEDM.

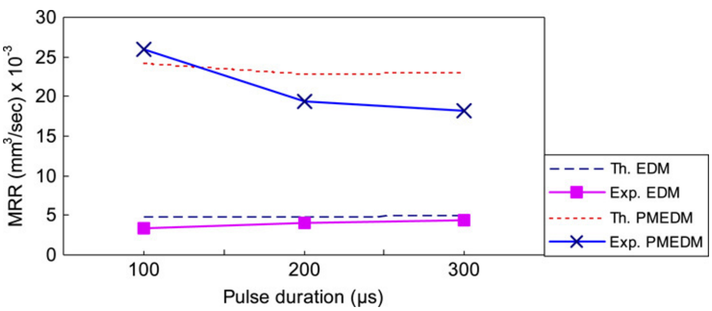

Fig. 20. Comparison between theoretical and experimental MRR for EDM and PMEDM.

5. Machining mechanism of PMEDM

On the basis of the results discussed for temperature distribution in the PMEDMed workpiece, the machining mechanism for PMEDM is proposed.

A schematic diagram of the proposed mechanism of material removal in PMEDM is illustrated in Fig. 21. When a voltage of 80–320 V is applied to both the electrodes, an electric field in the range 10^5–10^7 V/m is created. The spark gap is filled up with additive particles and the gap distance between tool and the workpiece increases from

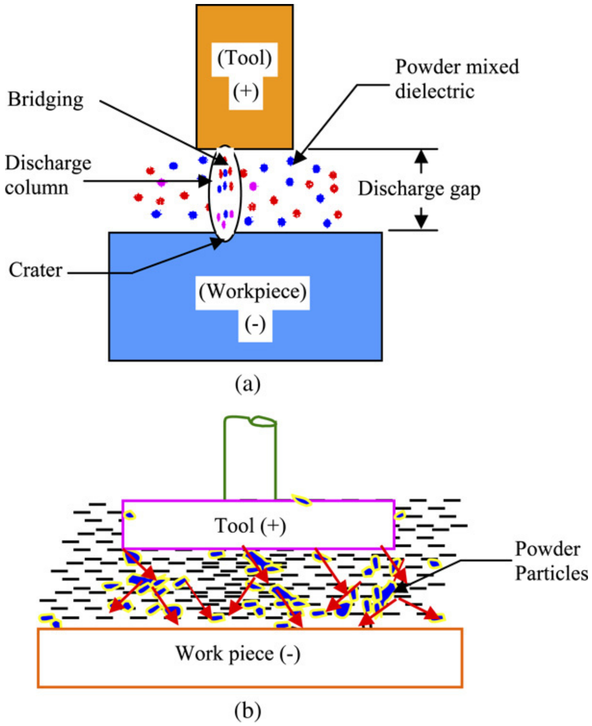

Fig. 21. Schematic representation of machining mechanism of PMEDM. (a) It is expected that the insulating strength of the dielectric fluid decreases as powder is suspended into it. The spark gap distance is increased by many folds than normal EDM. It is proposed that the increase in gap might have caused wider discharge passages. (b) In a wider and enlarged plasma channel, the suspended powder particles share and redistribute the impact force. As a result, shallow, uniform and flat craters are formed on the workpiece surface.

25–50 μm to many times as shown in Fig. 21(a). The powder particles get energized and behave in a zigzag fashion. The grains come close to each other under the sparking area and gather in clusters. Under the influence of electric forces, the powder particles as shown in Fig. 21(b), arrange themselves in the form of *chains* at different places under the sparking area. The chain formation helps in bridging the gap between both the electrodes. Due to the *bridging effect*, the gap voltage and insulating strength of the dielectric fluid decrease. The easy short circuit takes place, which causes early explosion in the gap. As a result, the *'series discharge'* starts under the electrode area. Due to increase in frequency of discharging, the faster sparking within a discharge takes place which causes faster erosion from the work piece surface. At the same time, the added powder modifies the plasma channel. The plasma channel becomes enlarged and widened [5]. The electric density decreases; hence sparking is uniformly distributed among the powder particles. As a result, even and more uniform distribution of the discharge takes place, which causes uniform erosion (shallow craters) on the workpiece. This results in an improvement in surface finish.

6. Conclusions

In this research paper, an axisymmetric two-dimensional thermal model was developed to predict the several aspects of the PMEDM. Numerical calculations and experiments have been done to analyze and compare the performance of EDM with PMEDM. The important features of the process such as temperature-sensitive material properties, shape and size of heat source (Gaussian heat distribution), percentage distribution of heat among tool, workpiece and dielectric fluid, pulse on/off time, material ejection efficiency and phase change (enthalpy) are taken into account in the development of the model. Finite element method (FEM) has been used to analyze the temperature profiles and material transformations that occur in the workpiece material due to high temperature, large deformations and transient operation. The FEM based model has been developed and solved using software ANSYS. The simulation results show that the PMEDM produces smaller and shallower craters than EDM under the same set of machining conditions. The effect of various process parameters (such as current, pulse on time, pulse off time, energy partition and phase change) on temperature distribution for PMEDM has been analyzed. Further, from the temperature distributions, the MRR is predicted. To validate the model, the predicted theoretical MRR is compared with the experimentally determined MRR values. An excellent agreement between experimental and theoretical results has been obtained.

The model developed in this research study for PMEDM can be further used to obtain the temperature distributions, residual stress distributions, metal flow and surface cracks on the PMEDMed machined workpieces. This means that the model can be used as an industrial tool to predict the evolution of temperature, stress, strain and cracks that may occur on the surface of the PMEDMed machined workpieces. The follow-up publications will consider the effect of multisparks and effect of various process parameters on the residual stress distributions and surface cracks.

Acknowledgements

The authors would like to acknowledge the support of M/S Electronica Machine Tools Ltd. Pune, India. We are deeply thankful to Dr. V.K. Jain, Professor, Department of Mech. Engg; IIT Kanpur, Dr. B.K. Mishra, IIT Roorkee, Dr. V. Yadav, MNNIT, Allahabad and Er. Baljit Singh, PSEB for their guidance and expert comments in response to our queries and problems.

References

[1] O.A. Abu Zeid, On the effect of electro-discharge machining parameters on the fatigue life of AISI D6 tool steel, Journal of Materials Processing Technology 68 (1) (1997) 27–32.
[2] P. Koshy, V.K. Jain, G.K. Lal, Experimental Investigations into electrical discharge machining with a rotating disc electrode, Precision Engineering 15 (1) (1993) 6–15.
[3] J.S. Soni, G. Chakraverti, Machining characteristics of Titanium with rotary electro-discharge machining, Wear 171 (1–2) (1994) 51–58.
[4] Biing Hwa Yan, C.C. Wang, Han Ming Chow, Yan Cherng Lin, Feasibility study of rotary electrical discharge machining with ball burnishing for Al_2O_3/6061Al composite, International Journal of Machine Tools and Manufacture 40 (10) (2000) 1403–1421.
[5] W.S. Zhao, Q.G. Meng, Z.L. Wang, The application of research on powder mixed EDM in rough machining, Journal of Materials Processing Technology 129 (2002) 30–33.
[6] Y.F. Tzeng, C.Y. Lee, Effects of powder characteristics on electro discharge machining efficiency, International Journal of Advanced Manufacturing Technology 17 (2001) 586–592.
[7] H. Narumiya, N. Mohri, N. Saito, H. Otake, Y. Tsnekawa, T. Takawashi, K. Kobayashi, EDM by powder suspended working fluid, in: Proc. 9th International Symposium for Electrical Machining, CIRP, 1989, pp. 5–8.
[8] N. Mohri, N. Saito, M. Higashi, A new process of finish machining on free surface by EDM methods, Annals of CIRP 40 (1) (1991) 207–210.
[9] A. Erden, S. Bilgin, Role of impurities in electric discharge machining, in: Proc. 21st Int. Machine Tool Design and Research Conference, Macmillan, London, 1980, pp. 345–350.
[10] Q.Y. Ming, L.Y. He, Powder-suspension dielectric fluid for EDM, Journal of Material Processing Technology 52 (1995) 44–54.
[11] M. Kunieda, K. Yanatori, Study on debris movement in EDM gap, International Journal of Electrical Machining 2 (1997) 43–49.
[12] Y.F. Luo, The dependence of interspace discharge transitivity upon the gap debris in precision electro-discharge machining, Journal of Materials Processing Technology 68 (1997) 127–131.
[13] K Furutani, A. Saneto, H. Takezawa, N. Mohri, H. Miyake, Accertation of titanium carbide by electrical discharge machining with powder suspended in working fluid, Precision Engineering 25 (2001) 138–144.
[14] Yih-fong Tzeng, Chen Fu-chen, A simple approach for robust design of high-speed electrical-discharge machining technology, International Journal of Machine Tool & Manufacture 43 (2003) 217–227.
[15] R. Snoyes, F. Van Dijck, Investigations of EDM operations by means of thermo mathematical models, Annals of CIRP 20 (1) (1971) 35.
[16] C.C. Marty, Investigations of surface temperature in electro discharge machining, Transactions of ASME, Journal of Engineering for Industry (1977) 682–684.
[17] A. Erden, B. Kaftanoglu, Heat transfer modeling of electric discharge machining, in: 21st MTDR Conference, Swansea, 1980, pp. 351–358.
[18] S.T. Jilani, P.C. Pandey, Analysis and modeling of EDM parameters, Precision Engineering 4 (4) (1982) 215–221.
[19] D.D. DiBitonto, P.T. Eubank, M.R. Patel, M.A. Barrufet, Theoretical models of the electrical discharge machining process. I. A simple cathode erosion model, Journal of Applied Physics 66 (9) (1989) 4095–4103.
[20] M.R. Patel, A. Barrufet, P.T. Eubank, D.D. DiBitonto, Theoretical models of the electrical discharge machining process—II: The anode erosion model, Journal of Applied Physics 66 (9) (1989) 4104–4111.
[21] P.E. Eubank, M.R. Patel, M.A. Barrufet, B. Bozkurt, Theoretical models of the electrical discharge machining process. III. The variable mass, cylindrical plasma model, Journal of Applied Physics 73 (11) (1993) 7900–7909.
[22] R. Bhattacharya, V.K. Jain, P.S. Ghoshdastidar, Numerical simulation of thermal erosion in EDM process, IE (I) Journal-PR 77 (1996) 13–19.
[23] V. Yadav, V.K. Jain, P.M. Dixit, Thermal stresses due to electrical discharge machining, International Journal of Machine Tools and Manufacturing 42 (2002) 877–888.
[24] ANSYS Advanced analysis procedure manual, ANSYS 5.4, ANSYS Inc., Canonsburg, Pennsylvania © SAS IP, Inc.
[25] Shuvra Das, Mathias Klotz, F. Klocke, EDM simulation: Finite element-based calculation of deformation, microstructure and residual stresses, Journal of Materials Processing Technology 142 (2003) 434–451.

[26] K. Morgan, R.W. Lewis, O.C. Zienkiewicz, An improved algorithm for heat conduction problems with phase change, International Journal of Numerical Method Engineering 12 (7) (1978) 1191–1195.
[27] P. Shankar, V.K. Jain, T. Sundarajan, Analysis of spark profiles during EDM process, Machining Science Technology 1 (2) (1997) 195–217.
[28] D.S. Kumar, Heat and Mass Transfer, 10th edition, S.K. Kataria & Sons, Delhi, 2000.
[29] P. Madhu, V.K. Jain, T. Sundararajan, K.P. Rajurkar, Finite element analysis of EDM process, Processing of Advanced Materials 1 (1991) 161–173.
[30] H.P. Schulze, R. Herms, H. Juhr, W. Schaetzing, G. Wollenberg, Comparison of measured and simulated crater morphology for EDM, Journal of Materials Processing Technology 149 (2004) 316–322.
[31] R. Snoyes, F. Van Dijck, Plasma channel diameter growth affects stock removal, Annals of CIRP 21 (1) (1972) 39–40.
[32] A. Erden, Effect of materials on the mechanism of electric discharge machining (EDM), Transactions of ASME, Journal of Engineering Materials and Technology 108 (1983) 247–251.
[33] P.S. Ayyaswamy, G.C. Das, I.M. Cohen, Thermal and electrical characteristics of a 2D 'Tanh' conductivity arc, Journal of Applied Physics 49 (1) (1978) 160–165.
[34] I.M. Cohen, P.S. Ayyaswamy, T. Sundararajan, Effect of plug flow on the stability of 2D arcs, IEEE Transactions of plasma Science PS-8 (4) (1980) 390–394.
[35] Y.S. Wong, L.C. Lim, Iqbal Rahuman, W.M. Tee, Near-mirror-finish phenomenon in EDM using powder-mixed dielectric, Journal of Materials Processing Technology 79 (1998) 30–40.
[36] J. Kozak, M. Rozenek, L. Dabrowski, Study of electrical discharge machining using powder suspended working media, Proceedings of Institution of Mechanical Engineers, Part-B 217 (2003) 1597–1602.
[37] P. Pecas, Almedia E. Henriques, Emerging technologies in penetration EDM, O Molde 55 (2002) 26–36.
[38] Y. Uno, A. Okada, Surface generation mechanism in electrical discharge machining with silicon powder mixed fluid, International Journal of Electro Machining 2 (1997) 13–18.
[39] A. Papoulis, Probability Random Variables and Stochastic Processes, McGraw Hill, New York, 1991.
[40] C.S. Desai, J.F. Abel, Introduction to the Finite Element Method, 1st edition, CBS Publishers and Distributors, Delhi, 1987.